Japanese Journal of
Applied Physics

REGULAR PAPER

# Composition and acoustic properties in a cartilage phantom



Japanese Journal of Applied Physics **58**, SGGE21 (2019) **REGULAR PAPER**
https://doi.org/**10.7567/1347-4065/ab1a2d**

# Composition and acoustic properties in a cartilage phantom

Naotaka Nitta[1*], Masaki Misawa[1], and Tomokazu Numano[2]

[1]*Health Research Institute, National Institute of Advanced Industrial Science and Technology (AIST), Tsukuba, Ibaraki 305-8564, Japan*
[2]*Department of Radiological Science, Tokyo Metropolitan University, Arakawa, Tokyo 116-855, Japan*

[*]E-mail: n.nitta@aist.go.jp

Received November 9, 2018; accepted April 1, 2019; published online July 4, 2019

In this study, a cartilage phantom that can be used for verifications and calibrations of not only magnetic resonance imaging (MRI) apparatus but also ultrasonic diagnosis equipment for cartilage diagnosis in the future was fabricated. Acoustic properties of the phantom fabricated for MRI apparatus evaluation were measured, and it was verified whether the acoustic properties of the phantom are close to those of the normal cartilage, which are set as the target values. In addition, as the fundamental physical properties of the cartilage phantom, the Young's modulus and the density were also measured. As a result, a cartilage phantom that satisfies target values of transverse relaxation time (T2) and apparent diffusion coefficient (ADC), and a target value of speed of sound (SOS) could be fabricated. © 2019 The Japan Society of Applied Physics

## 1. Introduction

As the aging population increases, the quantitative evaluation of cartilage tissue characteristics will become important. For example, osteoarthritis (OA) is a typical disease of articular cartilage and it has been reported that the tension of collagen fiber surface layer gradually decreases with cartilage degeneration.[1–4)] These evaluations have been tried in various ways. As the in vitro assessment using the ultrasound, ultrasound microscope,[5–9)] speed of sound (SOS) measurement,[10–13)] attenuation measurement,[14)] reflected wave or backscatter wave analysis,[15–18)] elastography using static deformation,[19,20)] and elasticity evaluation utilizing a laser measurement of ultrasonic particle velocity,[21,22)] have been investigated. As the in vivo assessment using the ultrasound, roughness analysis of cartilage surface, thickness measurement, and power Doppler analysis have been investigated.[23–27)] As the minimally invasive approach, the reflected wave analysis using an intravascular ultrasound has been investigated.[28)] As a fully-noninvasive method of SOS measurement, the multimodal method using a magnetic resonance imaging (MRI) device and an ultrasound diagnostic equipment has been proposed.[29–31)]

On the other hand, in addition to the above diagnosis methods, since the regenerated cartilage in the regenerative medicine has been expected as the fundamental treatment of cartilage diseases, establishment of an evaluation method for its maturity is an important subject. Specific methods suited for the evaluations of regenerated cartilage might be required, and it is important to explore and establish an appropriate evaluation method using not only ultrasonic but also other applicable modalities. Based on such a viewpoint, in our previous study, in vivo measurements of the regenerated cartilage implanted on the back of rats was comprehensively conducted using X-rays, MRI, ultrasound, etc, and then the correlation with elastic moduli and biochemical properties was investigated, and the evaluation parameters suitable for maturity evaluation were explored.[32)] As a result, the parameter values to be reached as the matured regenerated cartilage were clarified. Especially, since transverse relaxation time (T2) and apparent diffusion coefficient (ADC) of MRI exhibited the highest correlation with sulfated glycosaminoglycans (sGAG) and type-II collagen quantifying the content of cartilage matrix, it was revealed that T2 and ADC strongly reflect the maturation of regenerated cartilage subcutaneously transplanted in rats.

In the future clinical evaluation, it is assumed that the maturation of regenerated cartilage is evaluated over time by using the MRI apparatus of different facilities. At this time, one of the most important things is the verification and calibration of differences between devices in different facilities. In such a case, the use of a phantom is useful. Therefore, we decided to fabricate a cartilage phantom with T2 and ADC values of the matured regenerated cartilage for the purpose of evaluating the MRI apparatus.[33,34)]

On the other hand, as mentioned at the beginning of this section, there are many works on ultrasonic measurements of not only the regenerated cartilage but also normal cartilage. Among them, the SOS is still expected to be useful parameters for evaluating cartilage properties due to the following reason. Important properties of cartilage can be assumed to be mainly load support capacity or elasticity of the type-II collagen and water retention ability depending on proteoglycan content. Therefore, the parameters to be evaluated in the cartilage are both elasticity and water content. Since the shear wave does not propagate in water and consequently the shear modulus mainly reflects the elasticity of collagen, the evaluation of water content by only shear modulus may be difficult. On the other hand, theoretically, since the SOS of longitudinal wave is mainly affected by the bulk modulus, the SOS of longitudinal wave has a potential to evaluate both elasticity and water content. If the above-mentioned phantom has the SOS value or acoustic properties close to the normal cartilage, it is useful for the verification and calibration of ultrasound devices for cartilage diagnosis in the future. So far, although several phantoms for MRI apparatus based on agarose have been fabricated and evaluated,[35,36)] there is no phantom considering dual use with the ultrasound device. In general, any phantom is used not only for cartilage evaluation but also for other applications such as the detection of vulnerable plaque[37)] and treatment evaluation,[38)] and is also useful for the performance evaluation of conventional equipment and the verification of new methods.

Therefore, in this study, as a progress from Ref. 34, the practicality of the cartilage phantom that can be used for verifications and calibrations of both ultrasound and MRI devices was investigated. Specifically, frequency

dependencies of acoustic properties (SOS and attenuation) of the phantom fabricated for MRI apparatus evaluation were measured, and it was verified whether the acoustic properties of the phantom are close to those of the normal cartilage. In addition, as the fundamental physical properties of the cartilage phantom, the Young's modulus and the density were also measured. Moreover, in order to evaluate the reproducibility of phantom fabrication, T2, ADC, SOS, attenuation constant and Young's modulus of five phantoms fabricated by the same method were measured, and the repeatability of these measured values were evaluated.

## 2. Design of the cartilage phantom

In the design of the cartilage phantom in this study, the regenerated cartilage shown in Ref. 32, which was fabricated for partial defects of joint cartilage or nasal augmentation, was assumed. The regenerated cartilage fabricated with 100% chondrocytes is regarded as a normal cartilage, and T2, ADC and SOS of that cartilage is set as the target value of the phantom. That is, based on the result of Ref. 32, T2 of 0.100 s, ADC of $1.50 \times 10^{-3}$ mm$^2$ s$^{-1}$, were selected as the target values of cartilage phantom. In addition, SOS of around 1570 m s$^{-1}$ was also selected as a target value of the cartilage phantom.

Although not shown in Ref. 32, the Young's modulus and the bending modulus of the regenerated cartilage fabricated with 100% chondrocytes were measured as 220 kPa and 149 kPa, respectively. That is, the difference between them was 71 kPa. From this result, since the elastic anisotropy of this model cartilage was regarded to be relatively small, the elastic anisotropy was neglected in the phantom design of this study.

## 3. Composition of the cartilage phantom

### 3.1. Base material

As a base material, a polyacrylamide gel (OST, Japan) was used considering the possibility of ultrasound application. First, by adjusting the concentration of acrylamide, phantoms with three types of Young's modulus (Base 1: 148 kPa, Base 2: 506 kPa, Base 3: 702 kPa) were prepared. Here, Young's moduli of the Base 1 to 3 were obtained on the basis of the gradient in the range of 20 to 30 N of the force-displacement curve, by using the method described in Sect. 3.2. And then T2 and ADC were measured by using an 2 T MRI apparatus (Biospec, Bruker, Germany). These measurement results are shown in Fig. 1. Figure 1(a) shows the T2 values of three-type gels and Fig. 1(b) shows the ADC values. While the ADC value in a gel of Base 2 is close to the target value described in Sect. 2, it was impossible to simultaneously satisfy the target value of T2. Figure 1(c) is the result of SOS measured by the pulse transmission method described in Sect. 4.1. It is confirmed that the SOS in the gel of Base 2 can reproduce the SOS close to the target value described in Sect. 2.

From these results, the gel of Base 2 was selected as a base material. That is, in the selected gel, while the values of ADC and SOS are close to the target values described in Sect. 2, respectively, only adjustment of T2 value is required.

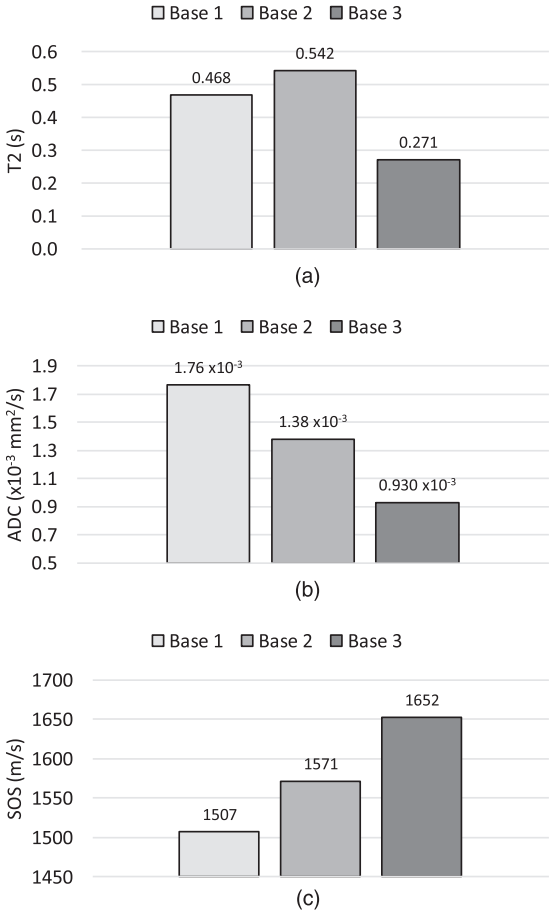


**Fig. 1.** Properties of base material candidates. (a) T2, (b) ADC, and (c) SOS. The significant figure of T2 and ADC is three digits.

### 3.2. Decision of the concentration of gadolinium-based contrast agent

Gadolinium-based contrast agents (GCAs) for MRI has an effect of shortening T2. Therefore, Magnevist®, which is a kind of the GCA for MRI, was diluted to ten kinds of concentrations (0, 0.5, 0.75, 0.85, 0.95, 1.05, 1.34, 1.62, 2.00, 2.50 mmol L$^{-1}$) and each diluted solution was uniformly mixed in the aforementioned polyacrylamide gel. Figure 2 shows the ten kinds of phantoms with different concentrations of GCA. Based on these phantoms, the shortening effect of T2 and the effect on other parameters were investigated. Here, each phantom has a plate-like shape and its dimensions are 50 mm × 50 mm × 10 mm.

Figures 3 and 4 show the measurement results of T2 and ADC, respectively. In Figs. 3, 3(a) is an example of T2 map and Fig. 3(b) is a graph of average value in the region of interest (ROI) of Fig. 3(a) to each concentration. As the concentration of GCA increased, the effect of shortening T2 was obtained. In Figs. 4, 4(a) is an example of ADC map and Fig. 4(b) is a graph of average value in the ROI of Fig. 4(a) to each concentration. Even if the concentration of GCA increased, the ADC remained almost constant. By using these properties, it is possible to fabricate a cartilage phantom that simultaneously satisfies the target values of T2 and ADC. That is, when the concentration of GCA is set to 0.85 mmol L$^{-1}$, a cartilage phantom that simultaneously satisfies T2 of 0.100 s and ADC of $1.50 \times 10^{-3}$ mm$^2$ s$^{-1}$ can be realized.

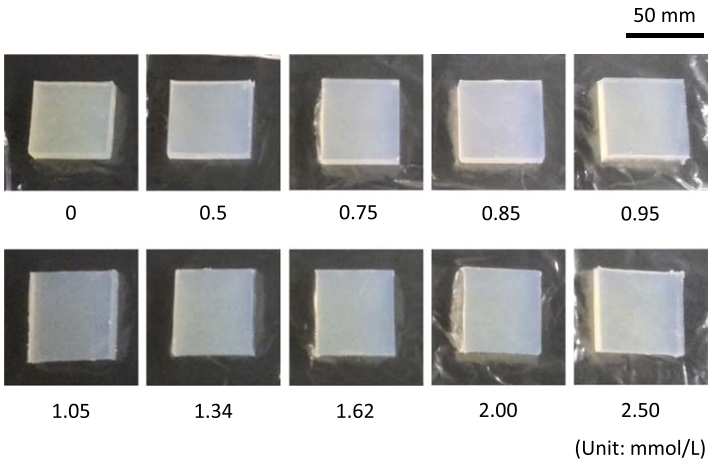


**Fig. 2.** (Color online) Cartilage phantoms with different concentrations of GCA. The number in the bottom of each photo indicates the concentration of GCA.

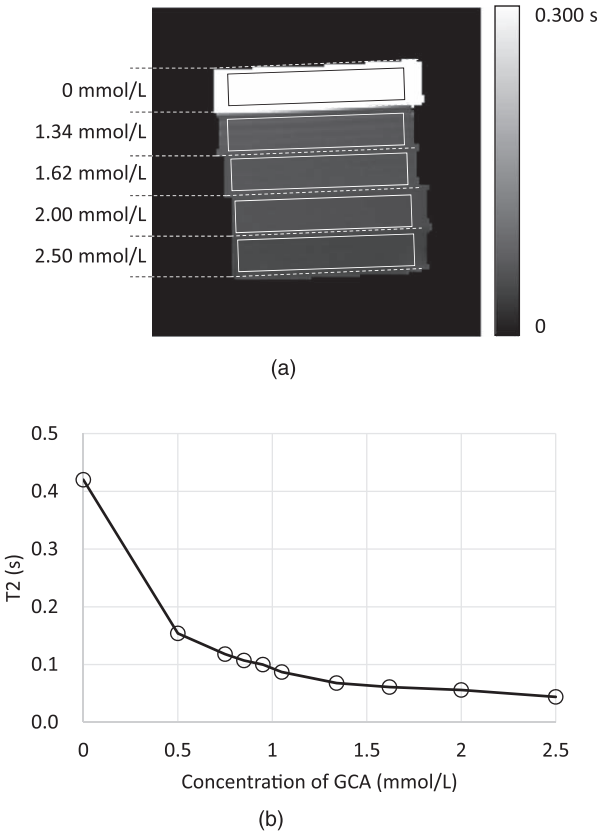


**Fig. 3.** T2 measurements of cartilage phantoms with different concentrations of GCA. (a) T2 map and (b) a relationship between average values of T2 in the region of interest (ROI) and GCA concentrations. Here, the broken lines depict the boundary of each phantom and the solid lines depict the ROI. The size of ROI is 42 × 7 mm. The significant figure of T2 is three digits. The grayscale of T2 map is assigned in the range of 0 to 0.300 s as a contrast adjustment for displaying all phantoms. Since 0 mmol $L^{-1}$ phantom at the top layer has T2 values over 0.300 s, its brightness is saturated.

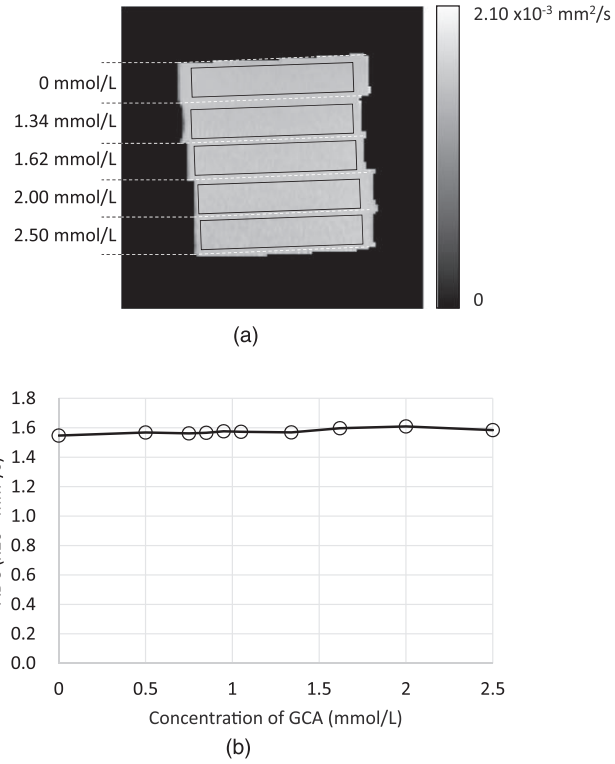


**Fig. 4.** ADC measurements of cartilage phantoms with different concentrations of GCA. (a) ADC map and (b) a relationship between average values of ADC in the region of interest (ROI) and the concentration of GCA. Here, the broken lines depict the boundary of each phantom and the solid lines depict the ROI. The size of ROI is 42 × 7 mm. The significant figure of ADC is three digits.

As fundamental physical properties, the density and the Young's modulus were measured. In the density measurement, first, the specific gravity of a phantom was measured by using a specific gravity meter (MD-300 s, Alpha Mirage, Japan). Then, by assuming that the density of water was 1 g $cm^{-3}$, the specific gravity was converted to the density. The Young's modulus was measured by a compression test using a universal testing machine (AG-500NX, Shimadzu, Japan). A circular compressor with a diameter of 50 mm was used, and the compression was conducted at a cross head speed of 1 mm per minute by using a load cell with a load capacity of 500 N and one-thousandth resolution. The plate-shaped phantom shown in Fig. 2 with a thickness of 10 mm was compressed in the thickness direction. The Young's modulus was calculated based on the gradient in the range of 20 to 30 N of the force-displacement curve and the dimensions of phantom. Here, the dimensions of phantom shape were measured by using a laser displacement meter (LK-G35, Keyence, Japan). Figure 5(a) shows the result of density measurement and Fig. 5(b) shows the result of Young's

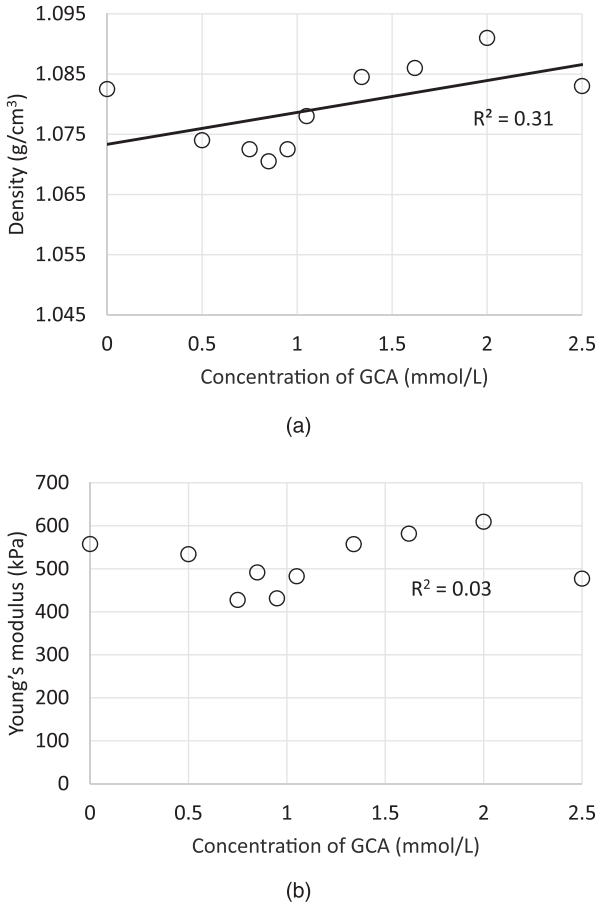


**Fig. 5.** Physical properties to the concentration of GCA. (a) Density and (b) Young's modulus.

modulus measurement. Since the density of GCA before dilution ($1.2\,\mathrm{g\,cm^{-3}}$) is higher than the density of polyacrylamide gel without GCA, the density of the whole phantom slightly increased with increasing concentration of GCA. On the other hand, no significant variations were observed in Young's modulus.

### 3.3. Reproducibility of phantom fabrication

In order to evaluate the reproducibility in fabricating the cartilage phantom that simultaneously satisfies T2 of 0.100 s and ADC of $1.50 \times 10^{-3}\,\mathrm{mm^2\,s^{-1}}$, five same phantoms satisfying the above T2 and ADC values were fabricated again. That is, the concentration of GCA was set to $0.85\,\mathrm{mmol\,l^{-1}}$. Then, T2 and ADC values of five phantoms were measured. As the result, the average value and standard deviation (SD) of T2 was $0.107 \pm 0.001$ s and the average value and SD of ADC was $1.57 \times 10^{-3} \pm 0.01 \times 10^{-3}\,\mathrm{mm^2\,s^{-1}}$. That is, the coefficient of variation (CV) of T2 and ADC corresponds to 0.9% and 0.6%, respectively. Therefore, the reproducibility of target values of T2 and ADC in fabricating the cartilage phantom can be assumed to be high.

In addition, the Young's moduli of these five phantoms were also measured. As the result, the average value and SD of Young's modulus was $488 \pm 22$ kPa. Since the CV of measured Young's modulus corresponds to 4.5%, the reproducibility of Young's modulus in the fabricated phantom can be also assumed to be relatively high. On the other hand, considering the minimum resolution of the load cell corresponds to 0.5 N and errors in the dimension measurement of phantom, the CV due to system resolution in the Young's modulus measurement can be estimated as 1.7%. Therefore, since the CV of measured Young's modulus is larger than the CV due to system resolution, most of the variation of measured Young's modulus can be suggested to be influenced by the variation of elasticity in the phantom fabrication process.

## 4. Measurement of acoustic properties

### 4.1. Speed of sound and attenuation constant measurement

**4.1.1. Setup.** For the measurements of SOS and attenuation constant, the pulse transmission method was used as shown in Fig. 6. In the transmission and the reception, non-focus circular transducers with a resonance frequency of 10 MHz and a diameter of 6 mm (126–340, GE Inspection Technologies, USA) were used. The frequency of 10 MHz is reasonable for clinical use and it is close to the frequency used in Ref. 32. The receiver (RE) is fixed in the bottom stage, and the transmitter (TR) is fixed by a holder attached at a linear stage, whose displacement is measured by a laser displacement meter (LK-G35, Keyence, Japan). This means that a distance between the surfaces of TR and RE is measurable. A sample (that is, a phantom) is sandwiched between TR and RE, but slight pushing occurs to ensure direct contact between the transducer surface and the phantom. In such a case, the distance between TR and RE can be regarded as equal to the thickness of the sample during the measurement of SOS and attenuation. Since the repetition precision of the laser displacement meter is 0.05 $\mu$m, consequently the thickness of the phantom can be precisely measured. The temperature of the entire phantom in measuring SOS and attenuation was kept at 23 °C.

**4.1.2. Data acquisition.** One-cycle sinusoidal wave generated by a function generator (AFG 3252, Tektronix, USA) was amplified by a power amplifier (150 W, R & K, Japan), and then applied to the transducer for transmission. The acoustic pressure at a distance of 5 mm apart from the surface of transducer was 0.45 MPa in water. Multiple reflections repeated at the boundary between the phantom and the transducer surface were recorded at a sampling frequency of 125 MHz and a quantization of 12 bit by using a digital oscilloscope (HDO 4034, LeCroy, USA). And then the SOS and attenuation constant were calculated as follows.

**4.1.3. Speed of sound.** For the multiple echoes including the first echo to the fourth echo, the arrival time of wavefront was read using waveform analysis software (WaveStudio, ver. 6.4.1.6, LeCroy, USA). However, this arrival time includes the delay of electric signal in the function generator. In order to remove the delay effect, the arrival time of wavefront and the propagation distance in multiple echoes are plotted as shown in Fig. 6(b), and the SOS is calculated from the gradient of the straight line. Because of the electrical signal delay, the intercept in Fig. 6(b) does not become zero. Considering the repetition precision (0.05 $\mu$m) of the laser displacement meter in measuring the thickness of the phantom, which is equal to the distance between TR and RE, and the reading error of 8 ns (sampling time) in measuring the arrival time, the error due to system resolution in the SOS measurement can be estimated as $0.5\,\mathrm{m\,s^{-1}}$, and this error corresponds to the CV of 0.03%.

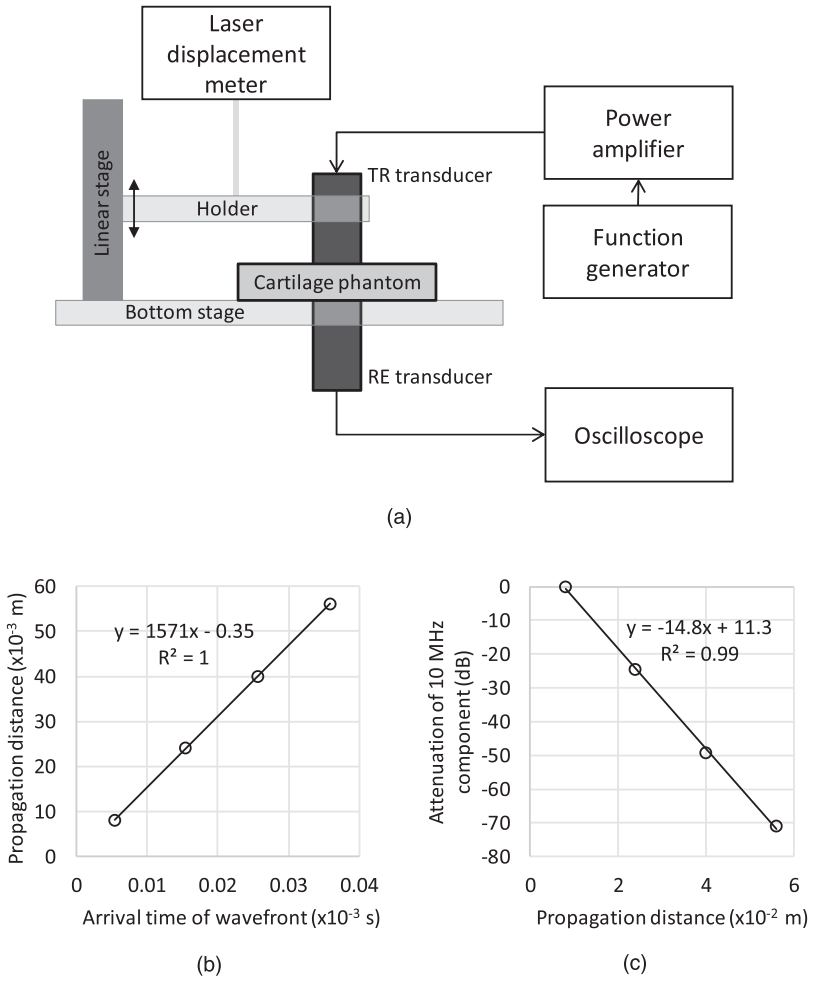


**Fig. 6.** (a) A measurement system for acoustic properties of a cartilage phantom. (b) shows a relationship between the propagation distance and the arrival time of wavefront for the SOS measurement, and (c) shows a relationship between the attenuation of 10 MHz component and the propagation distance.

**4.1.4. Attenuation constant.** When the amplitude of the 10 MHz component is obtained from each amplitude spectrum of the first echo to the fourth echo and normalized by the amplitude of the first echo, a linear relationship between the attenuation and the propagation distance can be obtained as shown in Fig. 6(c). Although the gradient $\alpha_p'$ of this straight line shows the apparent attenuation constant of the phantom, the reflection loss occurred at the boundary between the phantom and the transducer surface is included, as shown in Eq. (A.3) in the appendix. Therefore, by applying a correction method of the reflection loss shown in the appendix and calculating the reflectance $R_p$, the attenuation constant $\alpha_p$ of the phantom can be obtained without the reflection loss as follows

$$\alpha_p = \alpha_p' + \frac{\ln R_p}{l_p}. \quad (1)$$

Here $l_p$ is a distance between TR and RE.

### 4.2. Internal echo amplitude

B-mode images of all cartilage phantoms were acquired by using an ultrasound diagnostic device (EUB 8500, Hitachi, Japan), and the influence on the B-mode image due to the concentration of GCA was investigated.

## 5. Results

### 5.1. Speed of sound and attenuation

Figure 7(a) shows the measurement result of SOS and Fig. 7(b) shows the measurement result of attenuation constant. Although there was a tendency that the SOS slightly increased as the GCA concentration increased, no strong correlation was observed. From this result, it was confirmed that the SOS close to the target value of SOS described in Sect. 2 was reproduced almost independently of concentration of GCA. On the other hand, the relationship between the attenuation constant and the GCA concentration exhibited no significant correlation. As the results that SOS of five phantoms described in Sect. 3.3 were measured, the average value and SD of SOS was $1568 \pm 3\,\mathrm{m\,s^{-1}}$, and the CV was 0.3%. Therefore, the reproducibility of the target value of the SOS in fabricating the cartilage phantom can be assumed to be high. In addition, since the CV of measured SOS is larger than the CV due to system resolution described in Sect. 4.1.3, most variation of measured SOS can be suggested to be influenced by the variation of SOS in the phantom fabrication process.

Next, the frequency dependence of SOS and attenuation constant were measured, by using five cartilage phantoms described in Sect. 3.3. In the measurement system of Fig. 6, in addition to 10 MHz transducers described in Sect. 4.1.1,

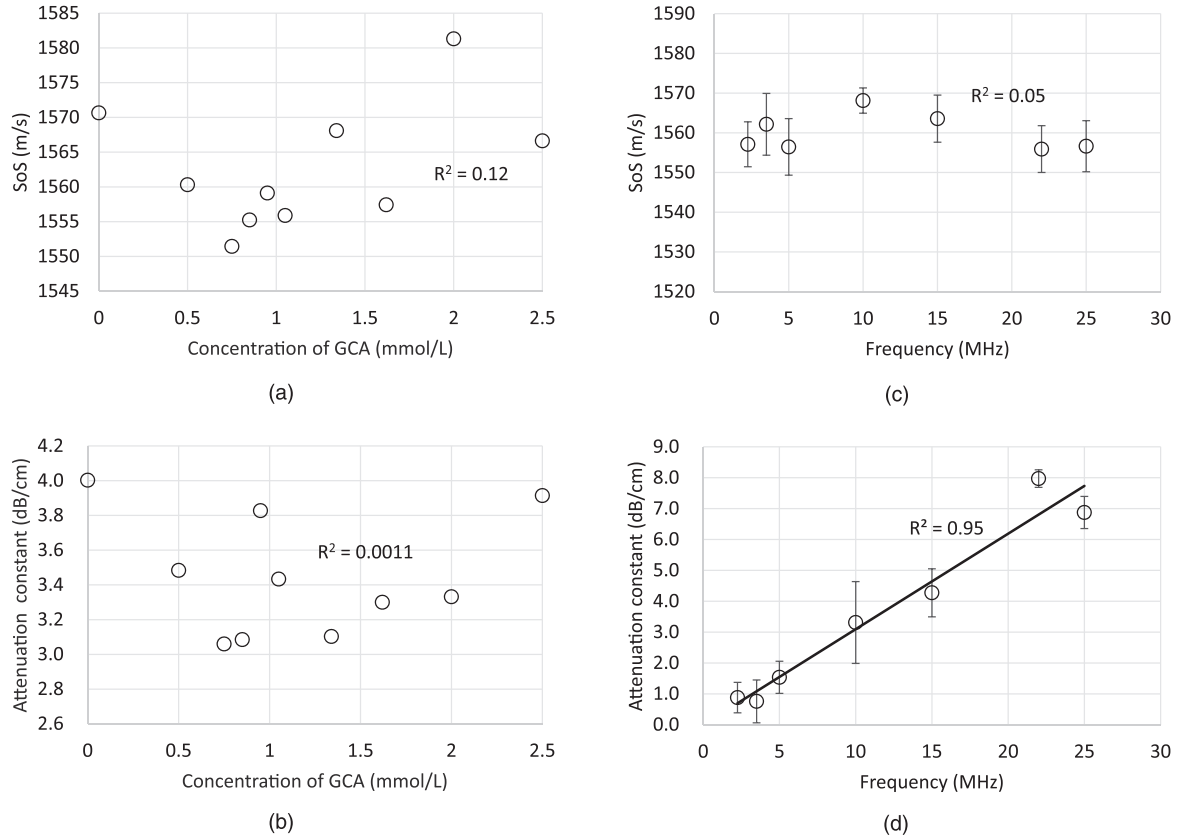


**Fig. 7.** Acoustic properties to the concentration of GCA. (a) SOS and (b) attenuation constant. (c) and (d) show the frequency dependence of SOS and attenuation constant of five cartilage phantoms under the same fabrication condition with the GCA concentration of 0.85 mmol $l^{-1}$, where the average value (depicted as a circle) and standard deviation (depicted as an error bar) are plotted.

other transducers with each resonance frequency of 2.25 MHz, 3.5 MHz, 5 MHz, 15 MHz, 22 MHz, 25 MHz were used. These transducers have the same manufacturer, aperture diameter and material of acoustic matching layer as the 10 MHz transducers. Figure 7(c) shows the result of measurement of the frequency dependence of SOS, where the average value and SD of five phantoms at each frequency are shown. Although the variation of SOS among five phantoms at each frequency was observed, no clear frequency dependence of SOS was found. The frequency dependence of attenuation constant is shown in Fig. 7(d). As the same as Fig. 7(c), the average value and SD of five phantoms at each frequency are shown. From this result, it was confirmed that the attenuation constant and the frequency are proportional in the cartilage phantom. Based on the gradient of straight line, the attenuation coefficient of 0.31 dB $cm^{-1}$ $MHz^{-1}$ was found. On the other hand, although not shown in Ref. 32, since the attenuation coefficient of the regenerated cartilage fabricated with 100% chondrocytes was 3.3 dB $cm^{-1}$ $MHz^{-1}$, the attenuation characteristics of the cartilage phantom were not fully reproduced.

### 5.2. Internal echo amplitude

Figure 8 shows the B mode image corresponding to each concentration of GCA. Here, the gain of all B mode images was kept constant. Figure 9 is a relationship between the average value of grayscale level (0 to 255) in a ROI of Fig. 8 and the concentration of GCA. It was observed that the average value of grayscale level in a ROI of B-mode image correlates with the concentration of GCA.

## 6. Discussions

In the introduction, it was described that the SOS of longitudinal wave has a potential to evaluate both elasticity and water content. On the other hand, the change in the SOS of the longitudinal wave when the elasticity changes may be too small to detect.[39] In order to verify this, a relationship between the SOS and the Young's modulus obtained from Figs. 5(b) and 7(a) is shown in Fig. 10. There was a moderate correlation between the SOS and the Young's modulus in the phantom. This result shows a possibility that the increase in the SOS of the longitudinal wave was induced by the increase in bulk modulus accompanied by the increase in Young's modulus due to the change of the physical properties. Although the relationship between the SOS of the longitudinal wave and the elasticity may depend on the kinds of material or biological tissue, the SOS of the longitudinal wave in this phantom can be an index suitable for evaluating the cartilage.

In this study, first, the concentration of polyacrylamide gel that satisfies a target value of ADC and SOS was determined, and then the concentration of GCA that satisfies a target value of T2 was determined. Based on this fabrication procedure, it was revealed that a cartilage phantom that simultaneously satisfies the target values of T2 and ADC could be fabricated, for verification and calibration of MRI apparatus. Furthermore, it became clear that the GCA concentration does not significantly affect on properties except for T2, and the SOS close to the target value is also maintained. From these results, it is also expected that the

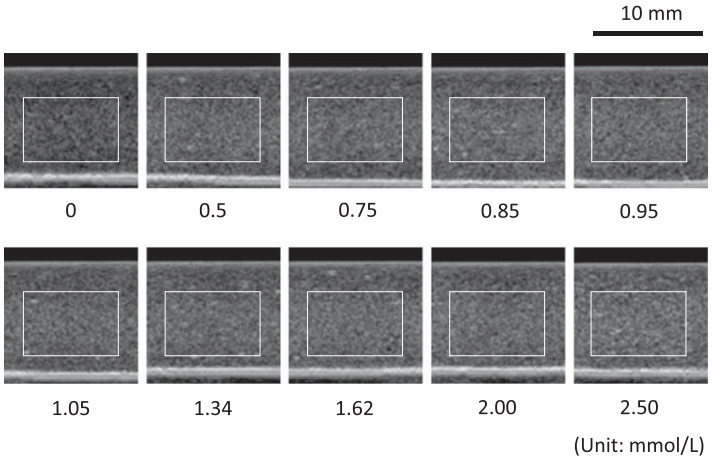


**Fig. 8.** The internal echo distribution of cartilage phantoms with different concentrations of GCA. The number in the bottom of each B mode image indicates the concentration of GCA. Here, the solid lines depict the ROI. The size of ROI is 9 × 6 mm.

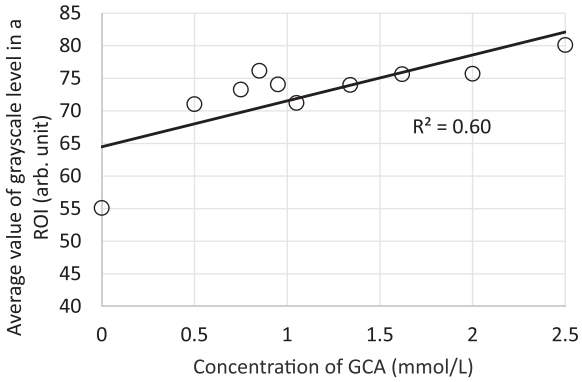


**Fig. 9.** A relationship between the average value of grayscale level (0 to 255) in a ROI of Fig. 8 and the concentration of GCA.

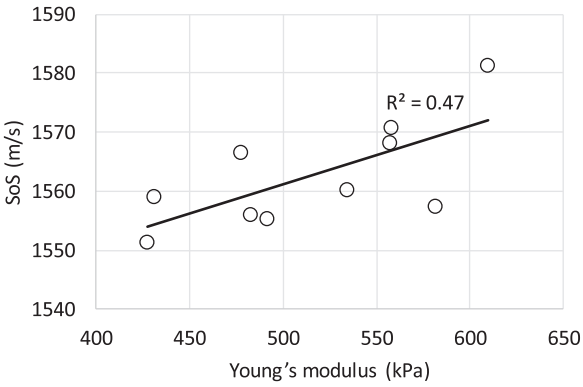


**Fig. 10.** A relationship between the Young's modulus and the SOS.

fabricated phantom can be used as a cartilage phantom for verification and calibration of the ultrasound diagnostic device for cartilage diagnosis in the future.

As described in Sect. 5.1, the SOS of the phantom fabricated under the same conditions exhibited a high reproducibility. On the other hand, in Fig. 7(a), slight variations according to the concentration of GCA were observed as SD of 9 m s$^{-1}$. Again, as with the prediction in Sect. 5.1, since the CV of measured SOS is larger than the CV due to system resolution described in Sect. 4.1.3, most variations of measured SOS can be suggested to be influenced by the variation of SOS in the phantom fabrication process. Specifically, the homogeneity of concentrations of acrylamide and GCA during the phantom fabrication process may affect on the variation of SOS. As an example of homogeneity evaluation, a relationship between the CV (ratio of SD to average value of ADC in a ROI) corresponding to the spatial variation of the ADC distribution in a ROI of Fig. 4 and the concentration of GCA is shown in Fig. 11. It was suggested that as the concentration of GCA increases, the CV increases and the homogeneity of ADC distribution tends to decrease. Consequently, the homogeneity of the SOS distribution may also decrease. Therefore, it is assumed that the above-mentioned slight variations of SOS were observed.

In Sect. 5.2, the increase of average value of grayscale level in a ROI of the B mode image, that is, the increase of brightness was observed according to the increase of the concentration of GCA. One possibility is that the heterogeneity of the SOS distribution affects on the increase of brightness. That is, as the concentration of GCA increases, the inhomogeneity of the SOS distribution increases, and consequently there is a possibility that the brightness is rising due to the change in the interference pattern.

Conversely, on the basis of Fig. 11, if the CV in the ADC distribution is 2.5% or less, the SD or the variation of SOS in the phantom fabrication process is expected to be suppressed within 9 m s$^{-1}$. On the other hand, in the verification and calibration process of an ultrasound device, a problem will be caused when the variation of SOS of a normal cartilage phantom exceeds the SOS of an abnormal cartilage.

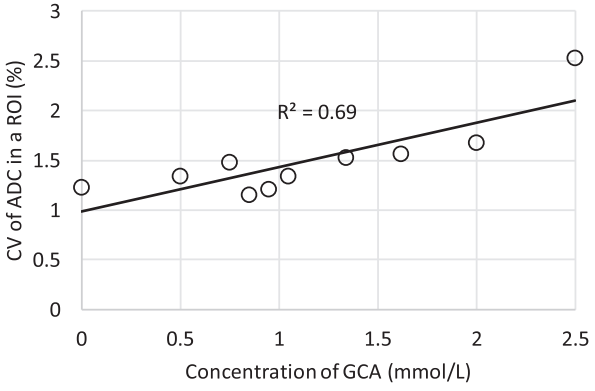


**Fig. 11.** A relationship between the concentration of GCA and the CV of ADC in a ROI.

However, as an example, when the SOS of the abnormal regenerated cartilage and the SOS of the normal regenerated cartilage shown in Ref. 32 were compared, the difference between them was in the range of 40 to 120 m s$^{-1}$. Needless to say, the variation of 9 m s$^{-1}$ is sufficiently smaller than the above difference. Therefore, in such a case, the variations of SOS that occur in the phantom fabrication process will not seriously affect the practicality of the phantom.

## 7. Conclusions

In this study, a cartilage phantom that satisfies the target values of T2 and ADC, and a target value of SOS was fabricated. From the results of this study, it is suggested that the cartilage phantom can be used not only for validation and calibration of MRI apparatus but also for verification and calibration of ultrasonic diagnostic equipment in the future. In future work, it is necessary to verify the temporal degradation of the cartilage phantom.

## Acknowledgments

This work was partly supported by a Health Labour Science Research Grant from the Ministry of Health Labour and Welfare, Japan.

## Appendix

Here, a method for correcting the reflection loss in the attenuation constant measurement is described. Assume that the acoustic impedance of the transducer surface material is unknown. In the measurement system of this paper, since the distance between TR and RE is almost 10 mm and it is within the Fresnel zone ($\leqslant a^2/\lambda$; $a$: a radius of circular transducer, $\lambda$: wavelength), diffusion attenuation can be neglected. At this time, in the multiple echoes occurring between TR and RE, a part of the acoustic pressure of reflection wave decreases repeatedly at the boundary of phantom and transducer surface due to the reflectance of acoustic pressure $R_p$. Therefore, the acoustic pressure $p_n$ of the resonance frequency component extracted from the $n$-th echo received at RE is described as follows.

$$p_n = R_p^{2(n-1)} p_0 e^{-\alpha_p (2n-1) l_p}. \tag{A.1}$$

Here, $p_0$ is an acoustic pressure when transmitting, $\alpha_p$ is an attenuation constant of the phantom, $l_p$ is a distance between TR and RE, that is, a thickness of the phantom. The logarithm of the ratio of $n$-th echo to first echo is written as follows.

$$\ln \frac{p_n}{p_1} = (\alpha_p l_p - \ln R_p) - (2n-1) l_p \left( \alpha_p - \frac{\ln R_p}{l_p} \right). \tag{A.2}$$

Here, $(2n-1)l_p$ indicates the propagation distance. Therefore, when plotting pairs of $\left((2n-1)l_p, \left(\frac{20}{\ln 10}\right) \ln \frac{p_n}{p_1}\right)$ ($n = 1$ to 4), Fig. 6(c) is obtained. At this time, the gradient $\alpha_p'$ of straight line in Fig. 6(c) is derived as follows.

$$\alpha_p' = \alpha_p - \frac{\ln R_p}{l_p}. \tag{A.3}$$

Therefore, the measured gradient $\alpha_p'$ is influenced by the reflectance $R_p$. In order to remove this reflection loss, a water tank was added to the measurement system of Fig. 6(a), and multiple reflection data in water were acquired under the same temperature as the phantom measurement. As with the phantom, a gradient as shown in Fig. 6(c) is obtained. However, considering that the diffusion attenuation is negligible and the absorption coefficient of water is almost zero, the gradient measured in the case of water $\alpha_w'$ is described as follows.

$$\alpha_w' \approx -\frac{\ln R_w}{l_w}. \tag{A.4}$$

Here, $R_w$ is the reflectance at the boundary of water and transducer surface, $l_w$ is a distance between TR and RE in water. By this relationship, $R_w$ can be obtained. The reflectance of acoustic pressure is determined by acoustic impedances of transducer surface material and sample material. Since the same transducers were used in both water and phantom measurements, the reflectance $R_p$ can be derived as follows.

$$R_p = \frac{R_w - \gamma}{1 - \gamma R_w}. \tag{A.5}$$

Here,

$$\gamma = \frac{Z_p - Z_w}{Z_p + Z_w}. \tag{A.6}$$

$Z_w$ and $Z_p$ are the acoustic impedance of water and phantom respectively, and these values were measured for water and all phantoms in this study. On the basis of these measurements, $R_p$ can be calculated. Then, by substituting $R_p$ into Eq. (1), the attenuation constant of the phantom without reflection loss can be obtained.

## ORCID iDs

Naotaka Nitta https://orcid.org/0000-0002-6036-4805
Masaki Misawa https://orcid.org/0000-0002-3685-5612

1) C. G. Armstrong and V. C. Mow, J. Bone Joint Surg. Am. **64**, 88 (1982).
2) J. S. Wayne, K. A. Kraft, K. J. Shields, C. Yin, J. R. Owen, and D. G. Disler, Radiology **228**, 493 (2003).
3) L. P. Li, W. Herzog, R. K. Korhonen, and J. S. Jurvelin, Med. Eng. Phys. **27**, 51 (2005).
4) L. P. Li, R. K. Korhonen, J. Iivarinen, J. S. Jurvelin, and W. Herzog, Med. Eng. Phys. **30**, 182 (2008).
5) Q. Wang and Y. P. Zheng, Ultrason. Med. Biol. **35**, 1535 (2009).
6) E. H. Chiang, T. J. Laing, C. R. Meyer, J. L. Boes, J. M. Rubin, and R. S. Adler, Ultrason. Med. Biol. **23**, 205 (1997).
7) M. H. Lu, Y. P. Zheng, and Q. H. Huang, Ultrason. Med. Biol. **31**, 817 (2005).
8) S. Z. Wang, Y. P. Huang, S. Saarakkala, and Y. P. Zheng, Ultrason. Med. Biol. **36**, 512 (2010).
9) Y. Tanaka, Y. Saijo, Y. Fujihara, H. Yamaoka, S. Nishizawa, S. Nagata, T. Ogasawara, Y. Asawa, T. Takato, and K. Hoshi, J. Biosci. Bioeng. **113**, 252 (2012).
10) H. J. Nieminen, P. Julkunen, J. Töyräs, and J. S. Jurvelin, Ultrason. Med. Biol. **33**, 1755 (2007).
11) J. K. F. Suh, I. Youn, and F. H. Fu, J. Biomech. **34**, 1347 (2001).
12) J. Töyräs, M. S. Laasanen, S. Saarakkala, M. J. Lammi, J. Rieppo, J. Kurkijärvi, R. Lappalainen, and J. S. Jurvelin, Ultrason. Med. Biol. **29**, 447 (2003).
13) S. G. Patil, Y. P. Zheng, and X. Chen, Ultrason. Med. Biol. **36**, 1345 (2010).
14) H. J. Nieminen, S. Saarakkala, M. S. Laasanen, J. Hirvonen, J. S. Jurvelin, and J. Töyräs, Ultrason. Med. Biol. **30**, 493 (2004).
15) A. S. Aula, J. Töyräs, V. Tiitu, and J. S. Jurvelin, Osteoarthritis and Cartilage **18**, 1570 (2010).
16) B. Pellaumail, A. Watrin, D. Loeuille, P. Netter, G. Berger, P. Laugier, and A. Saïed, Osteoarthritis and Cartilage **10**, 535 (2002).

17) S. Saarakkala, S. Z. Wang, Y. P. Huang, J. S. Jurvelin, and Y. P. Zheng, Ultrason. Med. Biol. **37**, 112 (2011).
18) K. Hattori, K. Mori, T. Habata, Y. Takakura, and K. Ikeuchi, Clinical Biomech. **18**, 553 (2003).
19) M. Fortin, M. D. Buschmann, M. J. Bertrand, F. S. Foster, and J. Ophir, J. Biomech. **36**, 443 (2003).
20) Y. P. Zheng, H. J. Niu, F. T. A. Mak, and Y. P. Huang, J. Biomech. **38**, 1830 (2005).
21) N. Nitta, M. Misawa, K. Homma, and T. Shiina, Jpn. J. Appl. Phys. **51**, 07GF15 (2012).
22) N. Nitta, K. Hyodo, M. Misawa, K. Hayashi, Y. Shirasaki, K. Homma, and T. Shiina, Jpn. J. Appl. Phys. **52**, 07HF24 (2013).
23) M. S. Laasanen, J. Töyräs, A. Vasara, S. Saarakkala, M. M. Hyttinen, I. Kiviranta, and J. S. Jurvelin, Osteoarthritis and Cartilage **14**, 258 (2006).
24) S. Saarakkala, J. Töyräs, J. Hirvonen, M. S. Laasanen, R. Lappalainen, and J. S. Jurvelin, Ultrason. Med. Biol. **30**, 783 (2004).
25) C. Y. Tsai, C. L. Lee, C. Y. Chai, C. H. Chen, J. Y. Su, H. T. Huang, and M. H. Huang, Osteoarthritis and Cartilage **15**, 245 (2007).
26) J. Töyräs, T. Lyyra-Laitinen, M. Niinimaki, R. Lindgren, M. T. Nieminen, I. Kiviranta, and J. S. Jurvelin, J. Biomech. **34**, 251 (2001).
27) L. Mancarella, M. Magnani, O. Addimanda, E. Pignotti, S. Galletti, and R. Meliconi, Osteoarthritis and Cartilage **18**, 1263 (2010).
28) T. Virén, S. Saarakkala, E. Kaleva, H. J. Nieminen, J. S. Jurvelin, and J. Töyräs, Ultrason. Med. Biol. **35**, 1546 (2009).
29) T. Aoki, N. Nitta, and A. Furukawa, Radiol. Phys. Technol. **6**, 480 (2013).
30) N. Nitta, T. Aoki, K. Hyodo, M. Misawa, and K. Homma, Proc. 35th Annual Int. Conf. IEEE Eng. Med. Biol. Soc., 2013, p. 6063.
31) N. Nitta, A. Kaya, M. Misawa, K. Hyodo, and T. Numano, Jpn. J. Appl. Phys. **56**, 07JF17 (2017).
32) Y. Fujihara et al., Tissue Eng. Part C: Methods **22**, 1 (2016).
33) N. Nitta, M. Misawa, and T. Numano, IEICE Technical Report **116**, 1 (2017), [in Japanese].
34) N. Nitta, M. Misawa, and T. Numano, Proc. 39th Symp. UltraSonic Electronics, 2018, p. 3P5.
35) J. R. McKinney, M. S. Sussman, R. Moineddin, A. Amirabadi, T. Rayner, and A. S. Doria, Clinics **71**, 404 (2016).
36) F. M. Buck, W. C. Bae, E. Diaz, J. Du, S. Statum, E. T. Han, and C. B. Chung, American Journal of Roentgenology **196**, W174 (2011).
37) Y. Kumagai, Y. Aotani, M. Kameda, K. Wada, T. Matsunaka, and H. Horinaka, Jpn. J. Appl. Phys. **57**, 07LF05 (2018).
38) D. Mashiko, S. Nishitaka, R. Iwasaki, M. Lafond, S. Yoshizawa, and S-I. Umemura, Jpn. J. Appl. Phys. **57**, 07LF13 (2018).
39) P. K. Choi, H. Takahashi, and Y. Onodera, IEICE Trans. A **J84-A**, 1439 (2001), [in Japanese].